

Periodic soliton trains and informational code structures in an improved soliton model for biomembranes and nerves

G. Fongang Achu, S. E. Mkam Tchouobiap, and F. M. Moukam Kakmeni*

Complex Systems and Theoretical Biology Group and Laboratory of Research on Advanced Materials and Non-linear Science (LaRAMaNS), Department of Physics, Faculty of Science, University of Buea, P.O. Box 63, Buea, Cameroon

C. Tchawoua

Laboratoire de Mécanique, Department of Physics, Faculty of Science, University of Yaoundé I, P.O. Box 812, Yaoundé, Cameroon



(Received 11 April 2018; published 20 August 2018)

Many experiments have shown that the action potential propagating in a nerve fiber is an electromechanical density pulse. A mathematical model proposed by Heimburg and Jackson is an important step in explaining the propagation of electromechanical pulses in nerves. In this work, we consider the dynamics of modulated waves in an improved soliton model for nerve pulses. Application of the reductive perturbation method on the resulting generalized Boussinesq equation in the low-amplitude and weak damping limit yields a damped nonlinear Schrödinger equation that is shown to admit soliton trains. This solution contains an undershoot beneath the baseline (“hyperpolarization”) and a “refractory period,” i.e., a minimum distance between pulses, and therefore it represents typical nerve profiles. Likewise, the linear stability of wave trains is analyzed. It is shown that the amplitude of the fourth-order mixed dispersive term introduced here can be used to control the amount of information transmitted along the nerve fiber. The results from the linear stability analysis show that, in addition to the main periodic wave trains observed in most nerve experiments, five other localized background modes can copropagate along the nerve. These modes could eventually be responsible for various fundamental processes in the nerve, such as phase transitions and electrical and mechanical changes. Furthermore, analytical and numerical analyses show that increasing the fourth-order mixed dispersion coefficient improves the stability of the nerve signal.

DOI: [10.1103/PhysRevE.98.022216](https://doi.org/10.1103/PhysRevE.98.022216)

I. INTRODUCTION

One of the most important and challenging problems in modern neuroscience is understanding the mechanism of excitation transmission in neurons [1–28]. To explain the experimental observation of the transmission of excitations of a given form over a large distance without noticeable deformation, the solitary-wave hypothesis has been successfully developed and proposed [1,2]. Solitary waves have been studied in a neural system, making it possible to describe the nonstationary-wave processes of energy, momentum, and information transmission through the neuron [1–10]. The idea of a neural signal being a mechanical solitary wave is not new. During the propagation of a neural signal, several mechanical or thermodynamical changes in the neuron and axon have been observed and demonstrated by cell swelling, heat release, changes in the fluorescence of membrane probes, turbidity, and birefringence [13–17]. In the early part of the 20th century, Wilke proposed that a nerve pulse is a pressure wave, and that the action potential is an epiphenomenon [18]. About 50 years later, Katz came up with the hypothesis that a neural signal is a single solitary pulse [19]. This solitary hypothesis gained more attention in the early 2000s, when Heimburg-Jackson proposed

a solitary model for a neural signal in the axon mediated by a phase transition [1].

Solitons are localized and self-sustaining waves that can propagate in a nonlinear dispersive medium without dissipating its energy [29,30], thus making them very useful in signal transmission. These nonlinear waves have been observed in many studies on neuronal systems. For instance, localized short impulses were observed in a nerve model with a self-excitable membrane [20]. Also, modulated waveforms were obtained numerically from the time series of the membrane potential derived from the dynamical mechanisms of waxing and waning oscillations in thalamic relay neurons [21], while self-sustained oscillations were reported in real neural tissue [22]. More recently [10], the multiple scale expansion method was used to show that the Hindmarch-Rose model of nerves includes localized nonlinear excitation. All of these studies report on the presence of nonlinear localized waves in a specific population of linked neurons under proper assumptions. In the Heimburg model of biomembranes and nerves, several forms of nonlinear excitations for a neural signal have been proposed [1,6,23]. In [1], an algebraic soliton solution for the nerve model traveling with the sound velocity along the axon was obtained. Contreras *et al.* [6] obtained analytically two forms of solutions for the Heimburg model of nerves. They proposed that in the gel state of the nerve, the Heimburg model includes bright solitons, while in the liquid state it includes dark solitons. They recently extended their work to obtain a compacton as a

*Author to whom all correspondence should be addressed: moukamkakmeni@gmail.com

possible profile for a nerve's signals [6]. Along the same lines, Vargas *et al.* obtained numerically localized periodic wave trains in the nerve model, thus explaining such nerve properties as hyperpolarization, pulse trains, and refractory periods. This provided a better explanation for the mechanism of periodic soliton trains with an intrinsic minimal distance between pulses of the order of about 5–10 pulse widths observed experimentally in the nerve of a locust [5]. However, to the best of our knowledge, a clear analytical picture describing these phenomena has not yet been established. It is also important to note that, in solid mechanics, the wave processes are fairly well understood [24], and the main point in wave dynamics is the concept of finite velocities—every excitation propagates with a finite velocity determined mainly by the properties of the medium [25]. This physical understanding has been well-reflected in the modified soliton model. However, there are still many questions to be answered, and research in this field, which includes the nature and structure of nerve pulses, is developing fast.

In the present study, an improved soliton model of biomembranes and nerves is used to establish that in a low-amplitude approximation, the dynamics of nerve impulses can be described by the damped nonlinear Schrödinger equation (DNLSE). Localized periodic wave trains will then be obtained, and their stability will be studied. Recall that in the cable model, as in the space clamp model, a constant low current stimulus leads to the generation of a single action potential. Higher current stimuli may generate infinite trains of action potentials [26]. Thus modeling the activity response to different neuronal geometries may shed light on the form-function interaction as a possible mechanism for information coding. Importantly, this type of solution is interesting in that it is observed during most nerve experiments and it contains nerve features such as wave trains, hyper-polarization, and a refractory period. Note that the main structural feature in nerve pulse dynamics is a stable solitary pulse of a characteristic asymmetric profile [25]. However, the bell shape is generally the one obtained by the linear stability analysis of this solution. We show that this well-known bell solution can copropagate with five other localized background modes. These modes might be responsible for various nerve processes, such as phase transitions and mechanical and/or electrical properties observed as secondary effects during nerve propagation. These background modes are also important in that they can be explored as a signature in explaining certain neurological diseases. Such diseases are characterized by an increase in neuronal activities, which results in undesirable sensory or motoric effects such as pain, abnormal muscle activity, spasticity, migraine, etc. For instance, as the main mode of propagation vanishes or minimizes during propagation along a nerve due to instabilities, information can be transmitted in the nervous system through background modes.

The structure of this work is as follows: In Sec. II, we briefly present the improved Heimburg-Jackson model and by using a reductive perturbation analysis in the low-amplitude limit, we examine modulated waves in the improved Heimburg-Jackson model; these waves appear as damped nonlinear Schrödinger solitons. In Sec. III, we obtain a bright solitary wavelike solution and localized periodic wave trains in the system. In Sec. IV, we examine the stability of localized periodic wave

trains. In Sec. V, we present a numerical analysis of the system. We end the work with discussion and conclusion in Sec. VI.

II. THE HEIMBURG-JACKSON MODEL REVISITED

A. The model

There are a number of mathematical models used to describe neural activity. These models include the Hodgkin-Huxley, Hindmarch-Rose, FitzHugh-Nagumo, and Heimburg-Jackson models. The Heimburg-Jackson model was recently improved by Engelbrech *et al.* [4]. Therefore, the improved Heimburg-Jackson model of nerve impulses is given by

$$\begin{aligned} \frac{\partial^2 \Delta \rho^A}{\partial t^2} = & \frac{\partial}{\partial x} \left((c_0^2 + \alpha \Delta \rho^A + \beta [\Delta \rho^A]^2) \frac{\partial \Delta \rho^A}{\partial x} \right) \\ & - H_1 \frac{\partial^4 \Delta \rho^A}{\partial x^4} + H_2 \frac{\partial^4 \Delta \rho^A}{\partial x^2 \partial t^2}, \end{aligned} \quad (1)$$

where the nerve axon is considered as a one-dimensional cylinder with lateral density excitations moving along the coordinate x and time t . $\Delta \rho^A = \rho^A - \rho_0^A$ is the change in the area density of the membrane as a function of x and t , ρ^A is the lateral density of a membrane, and ρ_0^A is the density of the membrane at physiological conditions, and it is slightly above the melting transition [1,5]. The parameters α and β describe the nonlinear elastic properties of membranes. At temperature slightly above the melting transition, the lipid membrane has negative values for the parameter α and positive values for the parameter β [5,9]. In fact, the ad hoc dispersive term $(\Delta \rho^A)_{xxxx}$ introduced to take into consideration the linear dependence of the pulse propagation velocity on frequency in [1] leads to unbounded velocities in higher frequencies, although the propagation of nerve impulses is said to be confined at lower frequencies. To avoid this anomalous dispersion, Engelbrech *et al.* [4] proposed a more realistic dispersive mechanism by adding a fourth-order mixed dispersive term $(\Delta \rho^A)_{xtxt}$ to the Heimburg-Jackson model. The numerical simulation showed that the combined terms satisfy the conditions for anomalous dispersion, and it is closed to physical experiments.

Note that when $H_2 = 0$, we have the Heimburg-Jackson model. In this specific case (i.e., $H_2 = 0$), it has been established that although the KdV equation describing the nerve pulse dynamics meets the required anomalous dispersion, the velocity of the propagating density pulse is not bounded for large values of the wave number [4]. This observation is in conflict with what is described in the Heimburg-Jackson model since all parameters defining the velocity remain finite [1]. The parameter H_2 was therefore added to the model to resolve this physically undesirable effect. Physically, the parameter H_2 represents the inertia of the lipid in the biomembrane, while H_1 represents the elasticity of the biomembrane, and both parameters are related to the nonlinear wave speed v at the high-frequency limit by $H_1 = v^2 H_2$ [4]. As pointed out in [5,27], a real nerve is not isolated but is viscously coupled to the surrounding fluids. Therefore, nerve compression, stretching, and friction can lead to the damping of the nerve's signal, hence the need to include the damping term $(\Delta \rho^A)_{xtt}$ in Eq. (1). Thus, the equation describing the dynamics of a nerve impulse in biomembranes and nerves, taking into account the effect of

damping, is given by

$$\begin{aligned} \frac{\partial^2 \Delta \rho^A}{\partial t^2} &= \frac{\partial}{\partial x} \left((c_0^2 + \alpha \Delta \rho^A + \beta [\Delta \rho^A]^2) \frac{\partial \Delta \rho^A}{\partial x} \right) \\ &\quad - H_1 \frac{\partial^4 \Delta \rho^A}{\partial x^4} + H_2 \frac{\partial^4 \Delta \rho^A}{\partial x^2 \partial t^2} + \vartheta \frac{\partial^2}{\partial x^2} \left(\frac{\partial \Delta \rho^A}{\partial t} \right). \end{aligned} \quad (2)$$

Equation (2) is a generalized Boussinesq equation with quadratic nonlinearity for the propagation of nerve impulses in a cylindrical biomembrane and nerve. For the data for dipalmitoyl phosphatidylcholine (DPPC) vesicles in the low-frequency case, Heimburg and Jackson obtained [1] $c_0 = 176.6$ m/s, $\alpha = \frac{-16.6c_0}{\rho_0^A}$, $\beta = \frac{79.5c_0^2}{(\rho_0^A)^2}$, $\rho_0^A = 4.035 \times 10^{-3} \frac{\text{g}}{\text{m}^2}$, and $H_1 = 2.225 \frac{\text{m}^4}{\text{s}^2}$, assuming a bulk temperature of $T = 45^\circ\text{C}$. On the other hand, $H_2 = 10^{-6} \text{m}^2$ [4].

In [1], Heimburg and Jackson have demonstrated that if the speed of the nonlinear waves is less than the speed of sound c_0 , then the solitary-wave solution to the KdV-like equation exists provided the nonlinearity balances the dispersion. Furthermore, under the same assumption, it has been established that if the speed of sound c_0 is equal to the speed of the propagating nonlinear waves v , then the soliton model admits algebraic solitons, while for $v \neq c_0$ it is possible to propagate subsonic and supersonic compactons [6]. Recall that all these solutions do not take into consideration the form of the main structural feature of nerve pulse dynamics. More recently, an attempt at this was proposed considering the effect of damping. It is demonstrated that if nonlinearity balances damping, then the Heimburg-Jackson model admits breathing soliton pulses, and under specific constraints these breathing pulses are self-trapped and travel along the nerve fiber with a constant profile even in the presence of damping [27]. In the following, we will show analytically that the extended model can propagate low-amplitude periodic wave trains observed during neuronal experiments.

B. The nonlinear amplitude equation

Equation (2) is a nonlinear partial differential equation, and it is difficult to handle using linear methods or direct numerical simulation. To find the solution of this equation, we must first obtain a useful and manageable equation by simplifying it while preserving the essential features of the system. This can be done using perturbation analysis. Some of these perturbation methods include regular perturbation analysis, the Stokes-Poincaré frequency-shift method, and the method of multiple scale expansion. The multiple-scale-expansion method is more robust in that it can work for a wide range of problems [10,27,29,30]. The main idea behind it is to introduce fast and slow variables into the equation. If we assume a low-amplitude oscillation of the density of the membrane, i.e., $\Delta \rho^A = \epsilon u$ ($\epsilon \ll 1$), and a weak damping such that $\vartheta \rightarrow \epsilon^2 \vartheta$, Eq. (2) can then be written as

$$\begin{aligned} \frac{\partial^2 u}{\partial t^2} &= c_0^2 \frac{\partial^2 u}{\partial x^2} + \frac{\partial^2}{\partial x^2} \left(\frac{\epsilon \alpha u^2}{2} + \frac{\epsilon^2 \beta u^3}{3} \right) \\ &\quad - H_1 \frac{\partial^4 u}{\partial x^4} + H_2 \frac{\partial^4 u}{\partial x^2 \partial t^2} + \epsilon^2 \vartheta \frac{\partial^2}{\partial x^2} \left(\frac{\partial u}{\partial t} \right). \end{aligned} \quad (3)$$

This equation has different solutions under different constraints. Using the tanh method and the harmonic balanced method, it has been established that such an equation admits both kink and bell-shaped solitons [31,32]. The equation can be transformed to obtain a modified form of the KdV-Burgers equation by means of the reductive perturbation method [27,33]. Here, we apply the method of multiple scale expansion and proceed further by making a change of variables according to the new time and space scales as $X_i = \epsilon^i x$ and $T_i = \epsilon^i t$. It should be noted that the main reason for employing this method is to find a solution $\Delta \rho^A(x, t)$ depending on these new sets of variables as a perturbation series of functions. Thus, we should obtain a perturbation series of operators from these independent variables as

$$\frac{\partial}{\partial t} = \frac{\partial}{\partial T_0} + \epsilon \frac{\partial}{\partial T_1} + \epsilon^2 \frac{\partial}{\partial T_2}, \quad (4)$$

$$\frac{\partial}{\partial x} = \frac{\partial}{\partial X_0} + \epsilon \frac{\partial}{\partial X_1}. \quad (5)$$

Accordingly, we can express the solution u in the form

$$u = A e^{i\theta} + A^* e^{-i\theta} + \epsilon (B e^{2i\theta} + B^* e^{-2i\theta}), \quad (6)$$

where the amplitudes A and B as well as their respective corresponding complex conjugates A^* and B^* are functions of $(T_1, T_2, \text{ and } X_1)$; $\theta = (kX_0 - \omega T_0)$, where k is the normal mode wave number and ω is the angular velocity of the wave.

By substituting Eqs. (4), (5), and (6) into the low-amplitude improved Heimburg-Jackson model (3) and grouping terms in order of perturbation ϵ^0 , ϵ^1 , and ϵ^2 , the following results are obtained:

At the zeroth-order of approximation ϵ^0 , annihilation of terms in $e^{\pm i\theta}$ gives the dispersion relation of the form

$$\omega = \pm \sqrt{\frac{c_0^2 k^2 + H_1 k^4}{1 + H_2 k^2}}. \quad (7)$$

As expected, this is indeed a dispersion relation of a continuous model. Obviously, this axonal dispersion is related to the system parameters H_1 and H_2 . From Eq. (7), we can define two important quantities related to wave dynamics: the phase velocity c_p and the group velocity c_g , respectively, given by

$$c_p = \sqrt{\frac{c_0^2 + H_1 k^2}{1 + H_2 k^2}} \quad (8)$$

and

$$c_g = \frac{c_0^2 k + 2H_1 k^3 + H_1 H_2 k^5}{\omega(1 + H_2 k^2)^2}. \quad (9)$$

The velocity is bounded and approaches the value $(H_1/H_2)^{-1/2}$ as the wave number approaches infinity, which means that short waves do propagate in the improved Heimburg-Jackson model. This is not the case for the Heimburg-Jackson model in which $H_2 = 0$ (Fig. 1). Similar results have been obtained by Engelbrecht *et al.* [4] by substituting a harmonic wave form in the linearized version of Eq. (1). It was also shown that an anomalous dispersion relation is possible if and only if $H_2 < H_1$.

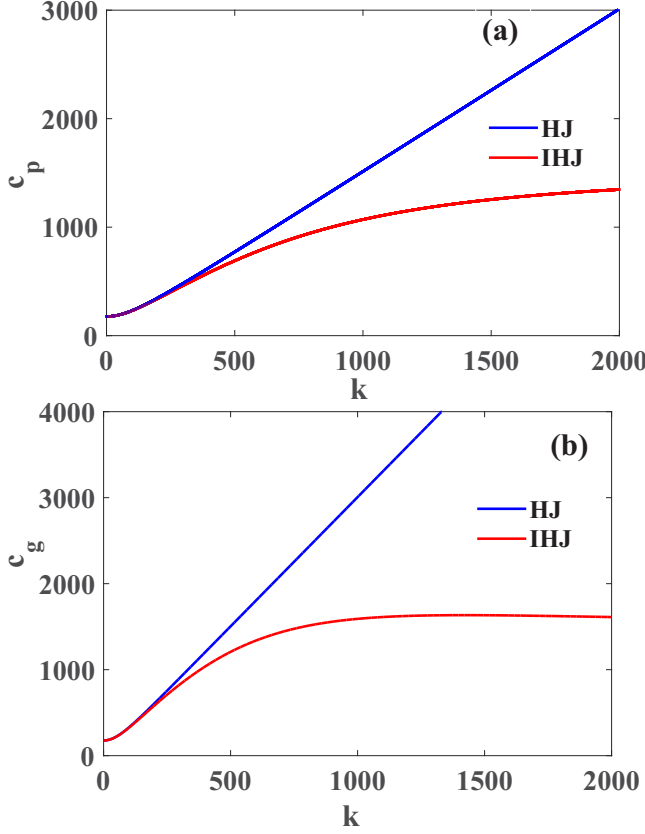


FIG. 1. The evolution of signal velocities against wave number: (a) Phase velocity for the Heimbürg-Jackson (HJ) and the improved Heimbürg-Jackson (IHJ) models. (b) The group velocity for HJ and IHJ $H_1 = 2.26 \text{ m}^4/\text{s}^2$ and $c_0 = 176.6 \text{ m/s}$. For the IHJ model, both the group and the phase velocity of the solitary wave have upper and lower cutoff speeds, thus the speeds are bounded.

Furthermore, at first-order perturbation, terms of order $e^{\pm 2\theta}$ give the relationship between the amplitudes A and B as

$$B = \frac{\alpha(1 + H_2 k^2)}{6(H_2 c_0^2 - H_1)k^2} A^2, \quad (10)$$

while at the second-order approximation ϵ^2 , an annihilation of terms in $e^{\pm i\theta}$ gives the damped nonlinear Schrödinger equation:

$$i \frac{\partial A}{\partial T_2} - \frac{P}{2} \frac{\partial^2 A}{\partial X_1^2} + Q|A|^2 A + iRA = 0, \quad (11)$$

with coefficients P , Q , and R , respectively, given by

$$P = \frac{4\omega c_g k H_2 + \omega^2 H_2 - c_g^2 - c_0^2 - 6H_1 k^2}{\omega(1 + H_2 k^2)}, \quad (12)$$

$$Q = \frac{\alpha^2(1 + k^2 H_2) - 6k^2 \beta (H_1 - H_2 c_0^2)}{12\omega(1 + H_2 k^2)(H_1 - H_2 c_0^2)}, \quad (13)$$

and

$$R = \frac{k^2 \vartheta}{2\omega(1 + H_2 k^2)}. \quad (14)$$

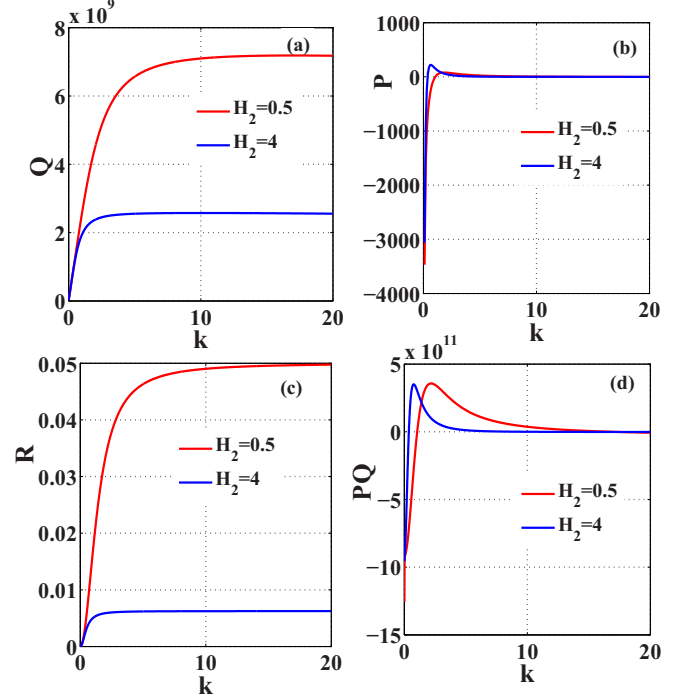


FIG. 2. Coefficients of the DNLS equation as a function of the wave number. (a) Nonlinear parameter Q , (b) dispersion coefficient P , (c) damping coefficient R , and (d) product PQ . The other model parameters are $c_0 = 176.6 \text{ m/s}$, $\alpha = -16.6c_0/\rho_0^A$, $\beta = 79.5c_0^2/(\rho_0^A)^2$, $\vartheta = 0.05$, $H_1 = 2.225 \text{ m}^4/\text{s}^2$, and $\rho_0^A = 4.035 \times 10^{-3} \text{ g/m}^2$. According to Benjamin-Fair instability, plane waves are unstable for positive values of PQ . Thus plane waves with wave numbers in the range $0.4 < k < 6$ and $0.6 < k < 17.2$ are unstable for inertia parameters $H_2 = 4$ and 0.5 , respectively.

The above damped nonlinear Schrödinger (DNLS) equation (11) is a canonical and universal equation that is of major importance in continuum mechanics, plasma physics, and optics. From a fundamental point of view, the DNLS equation permits us to investigate a traveling-wave profile characterized by an abrupt rise to the excited state and a drop back down to the refractory state, and periodic pulse generation observed in the soliton theory for nerves and experimentally in the locust femoral nerve [5]. Recent results on neural models clearly indicate that information encoding and transmission in the form of an electromechanical wave traveling along the axon can also emerge in the form of modulated structures [10,12,27].

As indicated in Fig. 2, the coefficient of the fourth-order mixed term H_2 strongly affects the nonlinear coefficient Q [Fig. 2(a)], the dispersion coefficient P [Fig. 2(b)], the damping coefficient R [Fig. 2(c)], and more importantly the product PQ [Fig. 2(d)]. All these parameters are plotted as a function of the wave number k for different values of H_2 . According to the Benjamin-Fair instability condition [54], plane waves are unstable if the product $PQ > 0$ and stable if $PQ < 0$. In Fig. 2(d), it is seen that, for $H_1 = 0.5$, plane waves are unstable for $0.6 < k < 17.2$; however, when the value of H_2 is larger, i.e., $H_2 = 4$, the instability region decreases, and the plane waves are now unstable for $0.4 < k < 6$. This result is important in the sense that stability plays a crucial role in

providing information on the local structure of the system. On the other hand, it is a crucial property of a wave profile in a neural network, since it determines whether such a pattern can be observed experimentally or utilized for diagnostic purposes [28]. Thus, in addition to setting a bound velocity for high frequency as predicted in [4], H_2 also improves the stability of the nerve signal. More importantly, the sign of PQ determines the nature of the solutions of Eq. (11). If PQ is positive, then Eq. (11) is said to admit a stable envelope soliton solution that has a vanishing amplitude as $|X_1| \rightarrow \infty$, and corresponds to a small-amplitude breathing pulse. However, if the product PQ is less than zero, then a dark (envelope hole) soliton will propagate with finite amplitude as $|X_1| \rightarrow \infty$ [27]. Thus, one expects to find in the nerve spatially localized nerve impulses for any wave carrier whose wave number is in the positive range of PQ .

III. THE DNLS EQUATION SOLUTIONS

Integrable and partially integrable inhomogeneous nonlinear Schrödinger equations have recently gained much popularity among mathematicians and physicists. While mathematicians are more concerned with developing methods for solutions to the equation, physicists focus their interests on special solutions that may fully describe and represent certain physical phenomena, which in our case is the structure of a nerve. Special solutions of extreme importance in the context of the present work are solitary-wave solutions, otherwise called solitons [10,27–29]. In this section, we focus on the well-known single-envelope soliton solution, and on periodic soliton trains. They are quite important in describing certain natural phenomena observed in the nervous system.

In the absence of damping (i.e., $R = 0$), Eq. (9) is simply a nonlinear Schrödinger equation. For the negative dispersion coefficient P and the positive nonlinear coefficient Q , the NLSE admits a modulated, localized envelope wave solution [27,29,30] in the form

$$A = A_0 \operatorname{sech} \left\{ \frac{X_1 - vT_2}{L} \right\} e^{i(kX_1 \pm \omega(k)T_2)}, \quad (15)$$

where L is the “hyperbolic secant” envelope width, and $\omega(k)$ and k are the modulation frequency and wave number, respectively. In this case, i.e., the DNLS equation, the question is what becomes of this soliton when R is nonzero. Several perturbation approaches have been developed to answer this question [34–38]. The perturbation technique developed for solitons includes the adiabatic perturbation method, the perturbed inverse scattering method, the Lie-transform method, and the variational method [39]. All these methods assume that the functional form of the soliton remains intact in the presence of a small perturbation, but the four soliton parameters change with time T_2 as the soliton propagates along the fiber. Thus, the soliton solution to the damped nonlinear Schrödinger equations becomes

$$A = A_0(T_2) \operatorname{sech} \{ A_0(T_2) [X_1 - k(T_2)] \} e^{i\phi(T_2) - i\sigma(T_2)}. \quad (16)$$

The T_2 dependences of A_0 , k , ϕ , and σ are determined through a set of four coupled ordinary differential equations for these four parameters obtained by injecting Eq. (16) into Eq. (11). In [40], using the variational approach, it was shown that for $R < 1$,

only the soliton amplitude A_0 and the phase ϕ are affected by the losses. Motivated by this result, and by the fact that we assume a very weak damping in the perturbation analysis, i.e., $\vartheta \rightarrow \epsilon^2 \vartheta$, the damped nonlinear Schrödinger equation can be transformed into an integrable equation by using the transformation $A = \psi \exp(-RT_2)$ [41,42] in Eq. (11), and one obtains

$$i \frac{\partial \psi}{\partial T} - \frac{P}{2} \frac{\partial^2 \psi}{\partial X^2} + \gamma |\psi|^2 \psi = 0, \quad (17)$$

where $\gamma = R_0 Q$, with $R_0 = |e^{-2(RT_2)}|$ denoting a normalized function. For simplicity of notation, we have also set $T = T_2$ and $X = X_1$. It should be emphasized here that for $R \ll 1$, $R_0 \approx 1$. The transformation ensures that only the amplitude and the phase of the solution are affected. It is noteworthy that Eq. (17) is the nonlinear Schrödinger equation. By setting

$$\psi(T, X) = \Gamma(X - u_e T) e^{i(X - \sigma T)} \quad (18)$$

and for positive P , Eq. (17) can be transformed to a first-order integral equation [43]:

$$(\Gamma')^2 = -\frac{P - 2\sigma}{P} \Gamma^2 + \frac{\gamma}{P} \Gamma^4 + C, \quad (19)$$

where C is the constant of integration, σ is the carrier speed, and $u_e = -P$ is the envelope speed. The constant C is important in determining the profiles of the temporal amplitude $\Gamma(Z = X - u_e T)$. To this extent, depending on the value of C , we can determine two types of profiles for the neural signal: a single soliton signal, which has been widely obtained both numerically and analytically under certain conditions [1,4–7], and soliton trains, which have been obtained numerically and experimentally [5]. Thus, in the following subsections, we examine these forms of solutions and discuss the conditions under which each solution is obtained, as well as their biological implications.

A. Single-envelope soliton signal of the DNLS of the system

More recently, by adding a small frictional term to the soliton model for nerves, breathing-type solitary-wave solutions were obtained [27]. Nevertheless, it is important to present the single-mode soliton solution. This will be compared later to the results derived in the form of a soliton train structure, which is one of the main focuses of the present work. For a localized profile, we expect a rapid evanescence of the wave outside its spatial bandwidth such that the constant C tends to zero [44–47]. Accordingly, this implies that the solution to Eq. (19) is obtained as

$$\Gamma(Z) = \sqrt{\frac{P - 2\sigma}{\gamma}} \operatorname{sech} \left\{ \sqrt{\frac{2\sigma - P}{P}} (Z) \right\}. \quad (20)$$

Thereby, the solution of the DNLS is given by

$$A = \sqrt{\frac{P - 2\sigma}{\gamma}} \operatorname{sech} \left\{ \sqrt{\frac{2\sigma - P}{P}} (Z) \right\} e^{i(X - \sigma T) - RT}. \quad (21)$$

It is important to note that the primary reason why we employ the multiscale analysis is to obtain low-amplitude modulated waves of the improved Heimbürg-Jackson model (3), and this solution is given by Eq. (6). As a consequence, by substituting

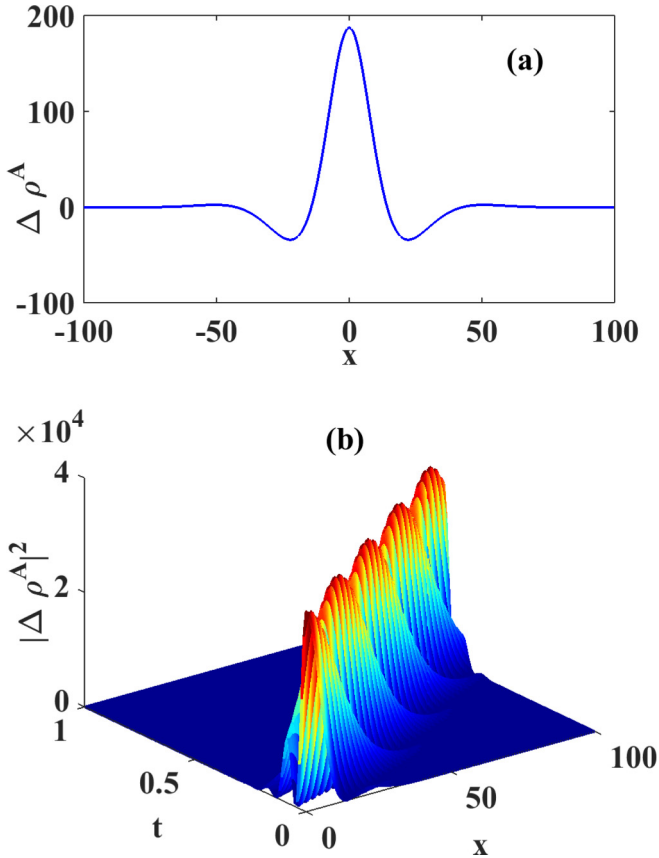


FIG. 3. (a) A typical single solitonlike signal predicted by Eq. (22); (b) the intensity of the change in the area density pulse $|\Delta\rho^A|^2$, corresponding to the square of the modulus of the evolution of a one-soliton waveform given by the change in the area density $\Delta\rho^A$. The parameters of the system are $H_1 = 2.26 \text{ m}^4/\text{s}^2$, $H_2 = 10^{-3} \text{ m}^2$, and $c_0 = 176.6 \text{ m/s}$, $\vartheta = 0.05$, $k = 0.03$, $\epsilon = 0.08$, and $\sigma = 100$. The single-envelope soliton solution has an undershoot beneath the baseline that represents the nerve signal phenomenon of hyperpolarization. It also propagates without changing its form, which is a typical characteristic of a solitary wave.

Eqs. (21) and (10) into (6) we obtain a solitonlike wave solution to the improved Heimburg-Jackson model as

$$\begin{aligned} \Delta\rho^A(x, t) = & 2\epsilon D_0 \operatorname{sech} \left\{ \sqrt{\frac{2\sigma - P}{P}} \epsilon(x - \epsilon u_e t) \right\} \\ & \times \cos(Kx - \Omega t) \\ & + 2 \frac{\epsilon^2 k \alpha (1 + k^2 H_2)}{3k^2 (H_2 c_0^2 - H_1)} D_0^2 \\ & \times \operatorname{sech}^2 \left\{ \sqrt{\frac{2\sigma - P}{P}} \epsilon(x - u_e t) \right\} \\ & \times \cos 2(Kx - \Omega t), \end{aligned} \quad (22)$$

where $\Omega = \omega - \epsilon^2 \sigma$, $K = \epsilon + k$, and $D_0 = \sqrt{\frac{P-2\sigma}{\gamma}} \exp\{-R\epsilon^2 t\}$.

It should be emphasized here that a similar solution has been obtained for $H_2 = 0$ [27]. Figure 3(a) is a graphical representation of a typical single solitonlike signal predicted

by Eq. (22). The intensity $|\Delta\rho^A|^2$ of the change in the area density pulse corresponding to the square of the modulus of the evolution of a one-soliton waveform given by the change in the area density $\Delta\rho^A$ is given in Fig. 3(b). This profile has an undershoot beneath the baseline, i.e., hyperpolarization, thus representing a typical nerve profile [5,27]. However, periodic trains as observed in most nerve experiments cannot be model using this solution. In the following subsection, we will analyze a periodic solution for the system.

B. Periodic solution of the NLSE of the system

The single soliton solution obtained so far cannot successfully explain all the nerve's features, i.e., refractory periods and pulse trains. In the following section, we will seek an analytical solution that is capable of describing these features. It should be noted that, while Eq. (22) describes a single-envelope soliton signal, elliptic solitons are specific nonlinear nerve signals characterized by a periodic structure made up of a large number of localized signals (bright- or dark-profile solitons), arranged so as to form a "periodic lattice" of pulses [43–47]. Elliptic solitons can be generated via modulational instability (MI) [54]. MI is a phenomenon whereby a continuous wave signal becomes unstable in a nonlinear structure as the input signal increases [27].

When the constant of integration C in Eq. (19) is nonzero and negative, the power of the wave is reduced and the energetic conditions become detrimental to the stability of a single pulse. However, we can still find nonlinear solutions to the amplitude viz. [43–47]

$$\Gamma(Z) = \sqrt{\frac{P - 2\sigma}{\gamma(2 - \kappa^2)}} \operatorname{dn} \left\{ \sqrt{\frac{2\sigma - P}{P(2 - \kappa^2)}}(Z), \kappa \right\}, \quad (23)$$

where dn is the Jacobi elliptical δ function of modulus κ ($0 < \kappa < 1$). As a consequence, the solution of the DNLS equation becomes

$$A = \sqrt{\frac{P - 2\sigma}{\gamma(2 - \kappa^2)}} \operatorname{dn} \left\{ \sqrt{\frac{2\sigma - P}{P(2 - \kappa^2)}}(Z), \kappa \right\} e^{i(X - \sigma T) - RT}. \quad (24)$$

Again, by substituting Eqs. (24), and (10) into (6), we obtain the solitary-wave solution to the improved Heimburg-Jackson model as

$$\begin{aligned} \Delta\rho^A(x, t) = & 2\epsilon D_0 \operatorname{dn} \left\{ \sqrt{\frac{2\sigma - P}{P(2 - \kappa^2)}} \epsilon(x - \epsilon u_e t), \kappa \right\} \\ & \times \cos(Kx - \Omega t) \\ & + 2 \frac{\epsilon^2 k \alpha (1 + k^2 H_2)}{3k^2 (H_2 c_0^2 - H_1)} D_0^2 \\ & \times \operatorname{dn}^2 \left\{ \sqrt{\frac{2\sigma - P}{P(2 - \kappa^2)}} \epsilon(x - u_e t), \kappa \right\} \\ & \times \cos 2(Kx - \Omega t), \end{aligned} \quad (25)$$

where $\Omega = \omega - \epsilon^2 \sigma$, $K = \epsilon + k$, and $D_0 = \sqrt{\frac{P-2\sigma}{\gamma(2-\kappa^2)}} \exp\{-R\epsilon^2 t\}$.

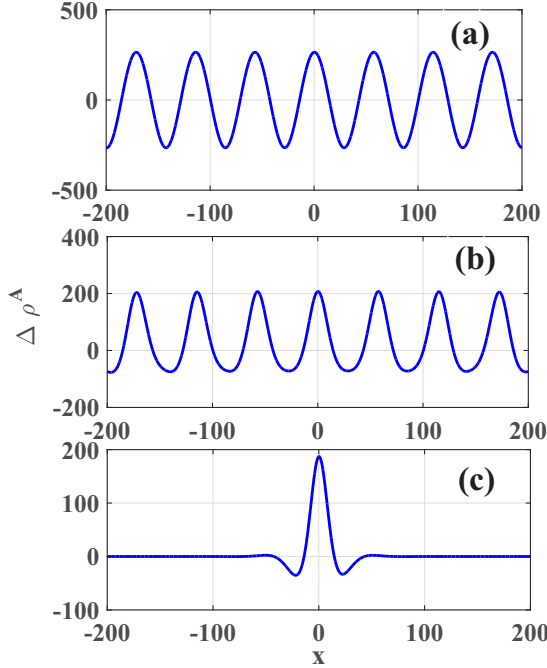


FIG. 4. Evolution of soliton trains in the system for different values of modulus κ : (a) $\kappa = 0$, (b) $\kappa = 0.88$, and (c) $\kappa = 1$ for $H_1 = 2.26 \text{ m}^4/\text{s}^2$, $H_2 = 10^{-3} \text{ m}^2$, and $c_0 = 176.6 \text{ m/s}$, $\vartheta = 0.05$, $k = 0.03$, $\epsilon = 0.08$, $\sigma = 100$, and $t = 0.01$. The soliton trains are separated from each other, which describes a nerve signal phenomenon of the refractory period. At $\kappa < 1$, the power of the wave is reduced and the energetic conditions are detrimental to the stability of a single pulse leading to a periodic soliton train.

Figure 4 illustrates the evolution of periodic wave trains describes by Eq. (25) for different values of the modulus of the elliptic function κ . It should be noted that for $\kappa = 1$, the periodic solution describes a single pulse [Fig. 4(c)] that is similar to the single-pulse profile (Fig. 3) described by Eq. (22). Most importantly, the solution (25) is more general and contains the solution (22) as a limiting case.

Also, we should note that Eq. (24) corresponds to the solution of the system when the second order of perturbation in Eq. (25) is set to zero. Thus, we can write for the first order of perturbation the solution to the system as

$$\Delta\rho^A(Z) = D_1 \operatorname{dn}\left\{\frac{Z}{Z_1}\right\} \cos(\theta_1), \quad (26)$$

where

$$Z_1 = \sqrt{\frac{P(2 - \kappa^2)}{2\sigma - P}} \epsilon \quad (27)$$

and

$$D_1 = 2R_1\epsilon \sqrt{\frac{P - 2\sigma}{\gamma(2 - \kappa^2)}}, \quad (28)$$

with $R_1 = \exp\{-R\epsilon^2 t\}$ representing the decay rate while $Z = x - \epsilon u_{\epsilon t}$ and $\theta_1 = Kx - \Omega t$. Here, the dn function is a periodic function of its argument Z , and it has recently been established that this function corresponds to a periodic

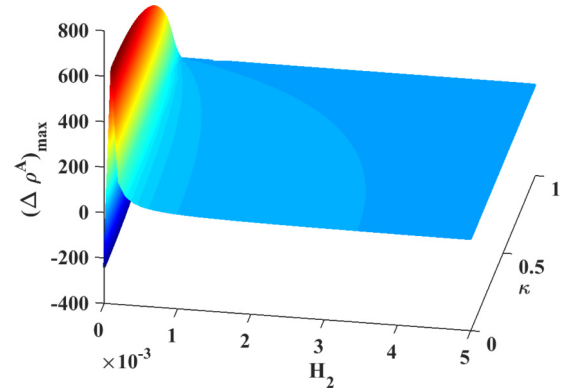


FIG. 5. The maximum amplitude of the train waves as a function of H_2 and κ . The other parameters are $H_1 = 2.26 \text{ m}^4/\text{s}^2$, $c_0 = 176.6 \text{ m/s}$, $\vartheta = 0.05$, $k = 0.03$, $\epsilon = 0.08$, $\sigma = 100$, and $t = 0.01$. The parameter space presents an initial increase in the amplitude for very small values H_2 and then an exponential decay as H_2 increases.

time-multiplexing of identical sech-type pulses to form a solitonic crystal of finite period $Z_2 = 2K(\kappa)Z_1$, where $K(\kappa)$ is the elliptic integral of the first kind [43]. Also, it should be noted that when $\kappa = 0$, the “dn” function is a “cw” field, and when $\kappa = 1$, the function reduces to the “sech” function as illustrated in Fig. 4. Since the period Z_2 tends to infinity in this later regime, the “dn” function can indeed readily be regarded as a train of pulses with a finite temporal separation between them. Similar results have been obtained numerically in the Heimburg-Jackson model and experimentally using the locust femoral nerve by Vargas *et al.* [5]. They demonstrated that the refractory period as well as the pulse trains and hyperpolarization in the soliton model appear as a consequence of the conservation of mass and the overall length of the nerve. An experimental demonstration with a locust femoral nerve depicts periodic patterns. These periodic pulses manifested themselves in the locust’s nerve as pulse “doublets,” and they display a constant distance of five to ten pulse widths even when measured under different conditions. It should be noted that an individual pulse width is 1–2 mm (or 1–2 ms). Moreover, similar pulse doublets and triplets have been observed in crayfish motor neurons [5].

Another property of soliton trains that is of importance is the maximum amplitude of the wave. This property can be used to predict the evolution of the wave with system parameters, and the corresponding structures are usually called bifurcation diagrams [48–51]. Indeed, we should recall that the argument of the dn function has a maximum value $K(\kappa)$ corresponding to $\sqrt{1 - \kappa^2}$ [52]. From this analysis, the maximum amplitude of the signal $[\Delta\rho^A(t)]_{\max}$ from Eq. (25) is given by

$$(\Delta\rho^A)_{\max} = 2\epsilon D_0 \sqrt{1 - \kappa^2} + 2 \frac{\epsilon^2 \kappa \alpha (1 + k^2 H_2)}{3k^2 (H_1 - H_2 c_0^2)} D_0^2 (1 - \kappa^2), \quad (29)$$

where $D_0 = \sqrt{\frac{P - 2\sigma}{\gamma(2 - \kappa^2)}} \exp\{-R\epsilon^2 t\}$.

The maximum $(\Delta\rho^A)_{\max}$ as a function of κ and H_2 is shown in Fig. 5. As can be seen in Fig. 5, the maximum amplitude increases linearly at small values of H_2 and

decreases exponentially for relatively large values of H_2 , i.e., $H_2 > 0.0002$. It is instructive to stress that, analogous to the information dimension, the Lyapunov exponents, and the Kolmogorov-Sinai entropy [53], the maximum value of the density pulse can be related to the optimal information that can be transmitted in the nerve. Hence, the maximum threshold value of $(\Delta\rho^A)_{\max} = 645$ corresponding to the inertia parameter $H_2 = 0.0002$ can be considered as the upper bound for the information production in the system. As a consequence, H_2 can be used to control the amount of information transmitted along the nerve fiber. It also characterizes the maximum compressibility of the membrane, which leads to the changes across the nerve cell membranes that convey information from one point to another in the nervous system. These sorts of changes are particularly important for the appearance of temporal patterns of action-potential activity and relating those patterns to stimulation by other inputs, or to specific behavioral events.

IV. STABILITY ANALYSIS OF THE SOLITON TRAINS

In the previous section, we obtained localized periodic wave trains in the improved Heimbürg-Jackson model. To discuss the stability of this solution, one must superimpose a small perturbation on this solution and analyze the evolution of the perturbation. Note that stability analysis is an important issue related to the study of nonlinear dynamical systems because it provides an effective way of testing the robustness of the soliton trains against small perturbation in the amplitude [54]. Because of the complexity of many physical problems, stability analysis is applied in a diverse manner. In this case, according to the linear stability analysis, the solution is considered to be of the form

$$A = \{A_0(X_1) + \epsilon A_1(X_1)\}e^{(i\sigma T_2 - RT_2)}, \quad (30)$$

where ϵ is a small parameter that separates the solution trains and the perturbation $A_1(X_1)$. After introducing this perturbed solution Eq. (30) into the DNLS equation (11), it is found that the solution and the perturbation obey the following equations at various orders of ϵ :

Order ϵ^0 ,

$$\frac{P}{2} \frac{\partial^2 A_0}{\partial X_1^2} - R_0 Q A_0^3 + \sigma A_0 = 0. \quad (31)$$

Order ϵ^1 ,

$$\frac{P}{2} \frac{\partial^2 A_1}{\partial X_1^2} - 3R_0 Q A_0^2 A_1 + \sigma A_1 = 0. \quad (32)$$

From Eq. (31), the solution at zeroth-order (ϵ^0) can be obtained by using the Jacobi elliptic dn function expansion method [43] as described previously, and it is given by

$$A_0(X_1) = \sqrt{\frac{2\sigma}{\gamma(2-\kappa^2)}} \text{dn} \left\{ \sqrt{\frac{-2\sigma}{P(2-\kappa^2)}} (X_1 - X_0) \right\}, \quad (33)$$

which is also a solution to Eq. (17).

As far as Eq. (32) is concerned, the divergence of the solution A_0 can only be prevented by finding the exact solution to Eq. (32) in A_1 . To obtain this solvability condition, we first use the transformation $Y = \lambda(X_1 - X_0)$ in (33) and substitute

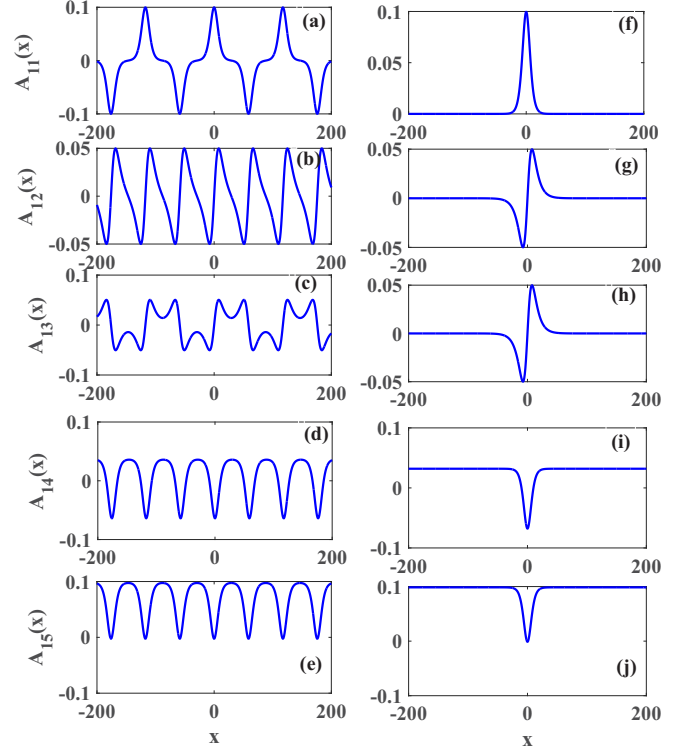


FIG. 6. Wave profiles of the five bound states A_{1j} ($j = 1, 2, 3, 4, 5$) for $\kappa = 0.98$ (a)–(e) and their corresponding profiles for $\kappa = 1$ (f)–(j). The other parameters are $H_1 = 2.26 \text{ m}^4/\text{s}^2$, $c_0 = 176.6 \text{ m/s}$, $\vartheta = 0.05$, $k = 0.03$, $\epsilon = 0.01$, $\sigma = 100$, and $t = 0.01$.

in Eq. (32), and the solvability condition of Eq. (32) can be expressed in term of Lamé's equation of the second kind as

$$\frac{\partial^2 A_1}{\partial Y^2} + (h(\kappa) - 6\kappa^2 \text{sn}^2(Y, \kappa))A_1 = 0, \quad (34)$$

where $h(\kappa) = \frac{6P\lambda^2 + 2\sigma}{P\lambda^2}$, with $\lambda = \sqrt{\frac{-2\sigma}{P(2-\kappa^2)}}$, and sn is another Jacobi elliptic function. Equation (34), which is sometimes referred to as a *secular equation*, has solutions A_1 that can copropagate in the nerve without influencing the system's dynamics. Thus the solution to the system will be stable if we can find the function $A_1(Y)$ such that Eq. (34) is satisfied. If there is no function $A_1(Y)$ that satisfies Eq. (34), then the solution $A = A_0 + \epsilon A_1$ will no longer be a solution to the DNLS Eq. (11), thus the solution A_0 will be unstable, or in other words, perturbed.

Lamé's equation, which has been widely studied [43–47,55], is an eigenvalue problem, and it possesses both discrete and continuous modes, all describing background modes of the localized periodic profile A_0 . This background wave has five distinct localized modes $A_1^j(Y)$ ($j = 1, 2, 3, 4, 5$) (see the Appendix). By transforming into original coordinates, i.e., $A_{1j} = A_1^j e^{(i\sigma T_2 - RT_2)}$, we plotted the five bound-state modes for two values of κ ($\kappa = 0.98$ [Figs. 6(a)–6(e)] and $\kappa = 1$ [Figs. 6(f)–6(j)]). These five bound-state solutions thus represent other profiles that can be obtained in the nerve. For instance, Figs. 6(g) and 6(h) represent a typical transverse profile obtained numerically in [4,56], while Figs. 6(i) and 6(j) represent a dark soliton profile obtained analytically in [6], and

it was explained that this profile of the nerve is possible at the fluid state. By contrast, Fig. 6(f) is the bright soliton profile and describes longitudinal propagation of a soliton in the gel state [1,6]. The five bound states can therefore be considered as the solitonlike structure that acts on the fluid motions in the elastic neuronal cells and fibers. They are thus the informational code structure releases in the form of impulses or pressure waves transmitted, and they cause the voltage changes across the nerve membrane, which are also well known to be the action potential. The above possible ensemble of waves emerging from these analyses demonstrates the complexity in signal propagation within neural systems. The propagation of the action potential is possible only in one of these modes, and it is mainly specified by the physical conditions. Following this, the behavior of biomembranes and nerves is an excellent example of the generation of multisolitons, which is interesting in the sense that it can be used to explain the enlarged capacity of communication channels existing in the nervous system. Indeed, as observed in Ref. [43], the formation of fundamental pulses in the NLSE is governed mainly by the balance of nonlinearity and the anomalous group-velocity dispersion. In this case, higher-energy pulses will split into identical lower-energy multisolitons (background modes) with exactly the same physical properties. Thus, the concept of background electromechanical neuronal impulses can be helpful to the understanding of other points of neurophysiology or neuronal diseases. For example, the propagation of these modes might be responsible for the structural changes of plasma proteins with coagulation phenomena or even for ruptures of the neuronal membranes, leading to diseases such as tangles and plaques, which are found, in particular, in senile and presenile dementia [57,59]. These plaques evolve from background modes that induce ruptures of neuronal cells or neuronal processes. They are created at an older age, and they reduce the resilience of the neuronal membranes, causing a reduced axoplasmic transport [57].

It is relevant to stress that the linear stability analysis provides a very efficient way of probing soliton stability, and particularly its shape invariance under translation. This issue has been investigated at length for single pulse and dark-soliton signals [58]. For single-soliton signals, the linear stability analysis of the wave equation (11) leads to an eigenvalue problem for which the discrete spectrum consists of three localized modes with nonzero temporal modulation. From a physics standpoint, these localized modes describe internal oscillations in the structure of the soliton signal that propagate with the signals. Because of their nonzero energies, they can be associated with radiation-carrying excitations in the propagating pulse background. From Figs. 6(g)–6(j), the single-pulse signal possesses three distinct localized modes, including a single-pulse, a symmetric two-pulse, and an asymmetric two-pulse bound state [45–47]. One of the three localized modes is precisely the translational mode, while the two others are related to localized excitations in the internal structure of the pulse due to its interaction with small-amplitude noise.

V. NUMERICAL EXPERIMENT

The results presented so far are just approximate because they were obtained after some hypotheses and considerations,

that is, the results are from the DNLS Eq. (11) rather than from the initial equation of motion (1). Furthermore, in order for these solutions to be reliable, it is always necessary to carry out direct numerical analysis. For this reason, the lifetime of the solutions determined above is an important parameter because only long-lived excitations can be detected experimentally. For the numerical integration, the Fourier-transform (FT)-based pseudospectral method (PSM) is used [4,60,61]. Note that the discrete FT based on the PSM with a hyperbolic sech function as an initial condition was also employed to solve the generalized Boussinesq Eq. (1) in [4]. Following this, before applying the PSM, one needs to ensure that the equation under consideration must be in a specific form, with only a time derivative on the left and spatial derivatives on the right [4,60,61]. By applying this method as proposed in [4], Eq. (1) is reduced to the following two first-order coupled differential equations:

$$\frac{\partial \Delta\rho^A}{\partial t} = F^{-1}\left(\frac{F(\phi)}{1 + H_2k^2}\right) \tag{35}$$

and

$$\begin{aligned} \frac{\partial \phi}{\partial t} = & c_0^2 F^{-1}((ik)^2 F(\Delta\rho^A)) \\ & \times F^{-1}\left(\alpha \frac{(ik)^2}{2} F((\Delta\rho^A)^2) + \beta \frac{(ik)^2}{3} F((\Delta\rho^A)^3)\right) \\ & - H_1 F^{-1}((ik)^4 F(\Delta\rho^A)) + \nu F^{-1}\left(\frac{F(\phi)}{1 + H_2k^2}\right), \end{aligned} \tag{36}$$

where F and F^{-1} are the FT and inverse FT, respectively. In what follows, the simulation is performed with a step size of $N = 200$ and an initial Jacobi dn function solution given by

$$\begin{aligned} \Delta\rho^A = & 10^{-4} \operatorname{dn}\left(\sqrt{\frac{\Lambda}{(2 - \kappa^2)}}x, \kappa\right) \cos\left(\frac{x}{10}\right) \\ & + 10^{-5} \operatorname{dn}^2\left(\sqrt{\frac{\Lambda}{(2 - \kappa^2)}}x, \kappa\right) \cos\left(\frac{x}{5}\right) \end{aligned} \tag{37}$$

and

$$\begin{aligned} \phi = & 10^{-3} \operatorname{sn}\left(\sqrt{\frac{\Lambda}{(2 - \kappa^2)}}x, \kappa\right) \\ & \times \operatorname{cn}\left(\sqrt{\frac{\Lambda}{(2 - \kappa^2)}}x, \kappa\right) \cos\left(\frac{x}{100}\right), \end{aligned} \tag{38}$$

where Λ is a constant. The other parameters use for the simulation are $H_1 = 2.25$, $\nu = 1.25$, $\alpha = -16.6 \frac{c_0^2}{\rho_0^A}$, $\beta = 79.5 \frac{c_0^2}{(\rho_0^A)^2}$, $c_0 = 176.6$, $dt = 0.001$, $\rho_0^A = 4.035 \times 10^{-3}$, $\kappa = 0.20$, and $\Lambda = 1.6 \times 10^{-3}$.

Now let us examine the effect of the fourth-order mixed derivatives H_2 on the soliton trains. Figure 7 presents the time evolution of periodic soliton trains for three different values of the dispersive coefficient H_2 . Accordingly, we observed that the number of soliton trains decreases as H_2 increases. Our numerical calculations also indicate that H_2 , which physically represents the inertia of the lipid membrane, determines the

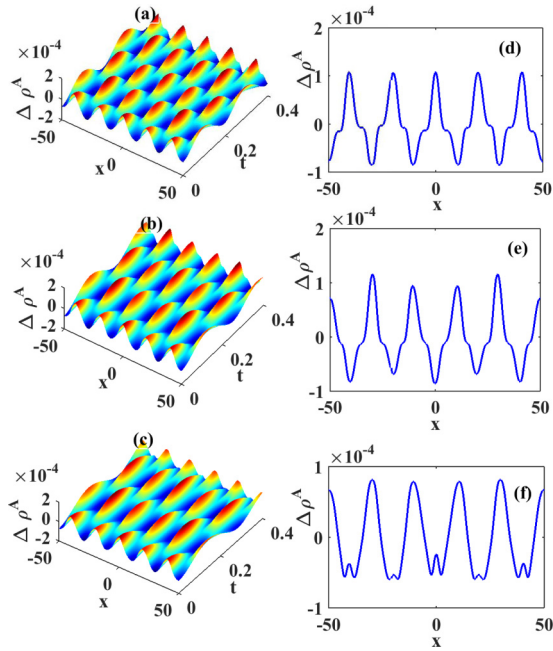


FIG. 7. Time evolution of periodic-soliton trains for different values of the dispersive coefficient H_2 . Parts (a) and (d) correspond to $H_2 = 0.4$, (b) and (e) correspond to $H_2 = 0.7$, while (c) and (f) correspond to $H_2 = 0.9$. The Jacobi elliptic function modulus is $\kappa = 0.4$.

localization of energy in the system. For large values of H_2 , the power of the wave increases, and the energetic conditions favor the propagation of more localized soliton trains.

Going ahead with our investigation, and as predicted by analytical results, κ also greatly affects the nature of the soliton profile, as can be seen in Fig. 8, where the evolution of the soliton trains is presented. Accordingly, Fig. 8 shows that soliton trains are not favorable as κ turns toward 1. More importantly, it should be mentioned that in [5], Vargas *et al.* transform the soliton wave equation for nerve dynamics into a classical wave equation comprised of kinetic and potential energy terms, and the integration constant C resulting from this transformation plays a critical rule in the evolution of the periodic pulses. However, in the present case the resulting NLSE obtained from the perturbation method admits similar periodic pulses. From Fig. 8, we observe that for $0 \leq \kappa < 1$, soliton trains are propagated along the nerve fiber, while for $\kappa = 1$ a single solitary pulse travels along the nerve. Thus, one can easily conclude that the Jacobi elliptic modulus κ determines the localization of energy along the nerve.

VI. DISCUSSION AND CONCLUSION

The key feature of the soliton theory for biomembranes and nerves is a localized pulse with constant entropy, i.e., without net heat exchange with the environment. Since the soliton theory is of a thermodynamic nature, any change in a thermodynamic variable that has the potential to move the membrane through its transition is also able to generate a pulse. This includes pulse generation by changes in temperature, voltage, lateral pressure, pH, calcium concentration, etc. In the soliton theory, a 2D sound propagating along the membrane

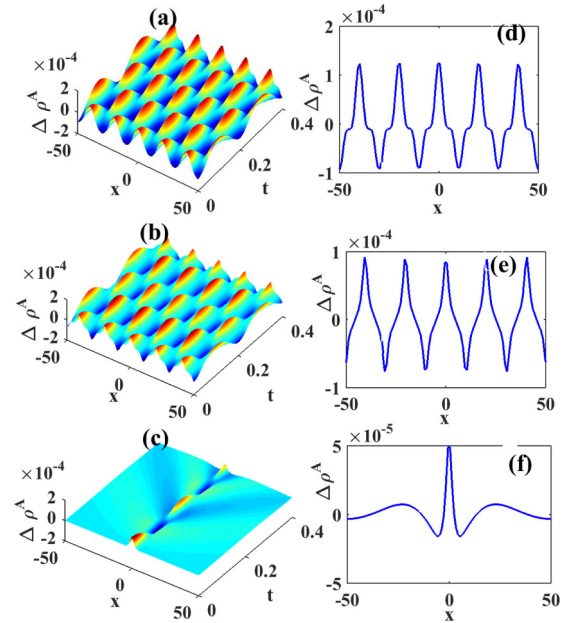


FIG. 8. Time evolution of periodic-soliton trains for different values of the Jacobi elliptic function modulus κ . Here, (a) and (d) correspond to $\kappa = 0.0$, (b) and (e) correspond to $\kappa = 0.98$, while (c) and (f) correspond to $\kappa = 1$. The dispersive coefficient is taken as $H_2 = 0.1$.

plane, described by lateral compressibility and a correlated change in density, is considered. By assuming an infinitely long axon that is quasi-one-dimensional, meaning that the thickness of the nerve is negligible compared to the length of the pulse, and that the density perturbation is of a longitudinal nature, Heimburg and Jackson considered the action potential as a 1D electromechanical pulse. The pulse consists of a locally compressed region in which the membrane is transiently pushed through its melting transition while releasing waves by spatial confinement [1,2,5]. The dynamical equation for the density pulses is a generalized Boussinesq-like equation with damping.

The soliton model is a true theory for a nerve pulse, based on the assumption of small friction. It describes why the pulse propagates and what its physical features are [27]. In contrast, El Hady and Machta considered a mechanical change caused by voltage pulses, but they did not explain from where a voltage-pulse originates [56]. By assuming a particular functional form of the *trans*-membrane voltage as in the Hodgkin-Huxley model, they deduced changes in the curvature and membrane thickness. In their calculations, the mechanical changes are side effects that do not couple back to the voltage changes from their description of mechanical changes. In the soliton theory, however, voltage change, mechanical changes, and temperature are just three different aspects of one phenomenon. Here, we have considered an improved soliton model for biomembranes and nerves, and it has solitary-wave excitations. In the low-amplitude limit and for weak damping, we used a multiple-scale analysis and established that the motion of nerve impulses is governed by the damped nonlinear Schrödinger equation (DNLS). The mixed fourth-order dispersion, which is physically related

to the inertia effects of the membrane structure, introduced important modifications in the nonlinear coefficient Q , the dispersion P , and damping parameters R . The phase and group velocity of the nerve signal are bounded due to the presence of the inertia term. Also, it is shown that in the improved Heimburg-Jackson model, these velocities converge to some maximum value $(\frac{H_1}{H_2})^{-1/2}$ as the wave number becomes very large, as described in [4]. This is not the case for the Heimburg-Jackson model. It was also noted that as H_2 increases, soliton trains become more localized, and H_2 can be used to control the amount of information transmitted along a nerve fiber.

Assuming a very weak damping, i.e., $R \ll 1$, a suitable transformation was used to change the nonintegrable damped nonlinear Schrödinger equation to a nonlinear Schrödinger equation. A single soliton signal as well as periodic wave trains of the nerve were obtained under specific conditions. It is shown that for a Jacobi elliptic function modulus of $\kappa = 1$, the nerve profile is a single soliton signal, and it is similar to the case obtained classically. The soliton train profile contains important features, such as hyperpolarization, a refractory period, and pulse trains, thus it can be used to model a neural signal. Linear stability analysis of the wave trains was also considered, and it was shown that in addition to the main localized periodic structure propagating along the nerve, five other bound-state modes can copropagate with it. In this way, it is suggested that these background modes may be responsible for some important nerve processes during neural activity, such as the flexoelectrical property of the cell membrane [62], ATP-induced reverse charge-transfer acceleration through helical proteins of the cell membrane [63,64], and more generally phase transitions involving the cell membrane [1,64]. Linear stability analysis might also be useful in explaining certain neural diseases, such as plaques and tangles in the brain [57]. Numerical analysis was also carried out to verify the analytical predictions.

ACKNOWLEDGMENTS

The authors thank A. M. Dikandé for useful discussions and for providing us with some of the materials used in the analysis of the present work.

APPENDIX

Bound-state solution of the Lamé equation

The five localized modes of the Lamé equation are given by

$$A_1^1(Y) = A_1^1(\kappa)\text{cn}(Y)\text{dn}(Y), \quad \sigma_1^1 = \{5 - \kappa^2\} \frac{|P|\lambda^2}{2}, \quad (\text{A1})$$

$$A_1^2(Y) = A_1^2(\kappa)\text{cn}(Y)\text{sn}(Y), \quad \sigma_{12} = \{2 - \kappa^2\} \frac{|P|\lambda^2}{2}, \quad (\text{A2})$$

$$A_1^3(Y) = A_1^3(\kappa)\text{sn}(Y)\text{dn}(Y), \quad \sigma_1^3 = \{5 - 4\kappa^2\} \frac{|P|\lambda^2}{2}, \quad (\text{A3})$$

$$A_1^4(Y) = A_1^4(\kappa) \left\{ \text{sn}^2(Y) - \frac{1 + \kappa^2}{3\kappa^2} - \frac{\sqrt{1 - \kappa^2(1 - \kappa^2)}}{3\kappa^2} \right\},$$

$$\sigma_1^4 = \left\{ 2 - \kappa^2 + \frac{\sqrt{1 - \kappa^2(1 - \kappa^2)}}{2} \right\} \frac{|P|\lambda^2}{2}, \quad (\text{A4})$$

$$A_1^5(Y) = A_1^5(\kappa) \left\{ \text{sn}^2(Y) - \frac{1 + \kappa^2}{3\kappa^2} + \frac{\sqrt{1 - \kappa^2(1 - \kappa^2)}}{3\kappa^2} \right\},$$

$$\sigma_1^5 = \left\{ 2 - \kappa^2 - \frac{\sqrt{1 - \kappa^2(1 - \kappa^2)}}{2} \right\} \frac{|P|\lambda^2}{2}, \quad (\text{A5})$$

where $A_1^j(\kappa)$ ($j = 1, 2, 3, 4, 5$) are their respective constant amplitudes.

[1] T. Heimburg and A. D. Jackson, *Proc. Natl. Acad. Sci. USA* **102**, 9790 (2005).
 [2] S. S. L. Andersen, A. D. Jackson, and T. Heimburg, *Prog. Neurobiol.* **88**, 104 (2009).
 [3] S. Shrivastava and M. F. Schneider, *J. R. Soc. Interf.* **11**, 20140098 (2014).
 [4] J. Engelbrecht, K. Tamm, and T. Peets, *Biomech. Model. Mechanobiol.* **14**, 159 (2015).
 [5] E. V. Vargas, A. Ludu, R. Hustert, P. Gumrich, A. D. Jackson, and T. Heimburg, *Biophys. Chem.* **153**, 159 (2011).
 [6] F. Contreras, H. Cervantes, M. Aguero, and M. D. L. Najera, *Int. J. Mod. Nonlin. Theor. Appl.* **2**, 195 (2013).
 [7] R. Appali, B. Lautrup, T. Heimburg, and U. Van Rienen, *Math. Ind.* **16**, 205 (2012).
 [8] B. Lautrup, R. Appali, A. D. Jackson, and T. Heimburg, *Eur. Phys. J. E* **34**, 57 (2011).
 [9] L. D. Mosgaard, A. D. Jackson, and T. Heimburg, *Adv. Planar Lipid Bilayers Liposomes* **16**, 51 (2012).
 [10] F. M. Moukam Kakmeni, E. M. Inack, and E. M. Yamakou, *Phys. Rev. E* **89**, 052919 (2014).
 [11] E. M. Yamakou, E. M. Inack, and F. M. Moukam Kakmeni, *Nonlin. Dyn.* **83**, 541 (2015).
 [12] F. M. Moukam Kakmeni and V. M. Nguemaha, *Phys. Lett. A* **380**, 200 (2016).
 [13] I. Tasaki, *Physiol. Chem. Phys. Med. NMR* **20**, 251 (1988).
 [14] B. C. Abbott, A. V. Hill, and J. V. Howarth, *Proc. R. Soc. London, Ser. B* **148**, 149 (1958).
 [15] J. M. Ritchie and R. D. Keynes, *Q. Rev. Biophys.* **18**, 451 (1985).
 [16] I. Tasaki and M. Byrne, *Biophys. J.* **57**, 633 (1990).
 [17] I. Tasaki, A. Watanabe, R. Sandlin, and L. Carnay, *Proc. Natl. Acad. Sci. USA* **61**, 883 (1968).
 [18] E. Wilke, *Pfluger. Archiv. Physiol. Mensch. Tiere* **144**, 35 (1912).
 [19] B. Katz, *Nerve, Muscle, and Synapse* (McGraw-Hill, New York, 1966).
 [20] A. M. Dikandé and G. A. Bartholomew, *Phys. Rev. E* **80**, 041904 (2009).

- [21] A. Destexhe, A. Babloyantz, and T. J. Sejnowski, *Biophys. J.* **65**, 1538 (1993).
- [22] Z. P. Kilpatrick and P. C. Bressloff, *Physica D* **239**, 547 (2010).
- [23] F. O. Larios, N. P. Tretyakov, and M. A. Agüero, *J. Nonlin. Dyn.* **2014**, 710152 (2014).
- [24] J. Miklowitz, *The Theory of Elastic Waves and Waveguides* (Elsevier Science, Amsterdam, 2012).
- [25] J. Engelbrecht, *Periodica Polytechnica. Ser. Mech. Eng.* **36**, 153 (1992).
- [26] N. Ofer and O. Shefi, *Appl. Math. Model.* **40**, 3175 (2016).
- [27] G. Fongang Achu, F. M. Moukam Kakmeni, and A. M. Dikandé, *Phys. Rev. E* **97**, 012211 (2018).
- [28] N. O. Nfor, P. G. Ghoms, and F. M. Moukam Kakmeni, *Phys. Rev. E* **97**, 022214 (2018).
- [29] M. Dauxois and M. Peyrard, *Physics of Solitons* (Cambridge University Press, Cambridge, 2006).
- [30] R. H. Enns, *It's a Nonlinear World* (Springer, New York, 2011).
- [31] P. Meng and W. Yin, *The Travelling Wave Solutions of KdV-Burger Equations*, International Conference on Management Science and Innovative Education (MSIE 2015), Vol. 399 (Atlantis Press, 2015).
- [32] M. Wung, *Phys. Lett. A* **213**, 279 (1996).
- [33] C. H. Su and C. S. Gardner, *J. Math. Phys.* **10**, 536 (1969).
- [34] V. I. Karpman and E. M. Maslov, *Zh. Eksp. Teor. Fiz.* **73**, 537 (1977) [*Sov. Phys. JETP* **46**, 281 (1977)].
- [35] D. J. Kaup and A. C. Newell, *Proc. R. Soc. London, Ser. A* **361**, 413 (1978).
- [36] V. I. Karpman, *Zh. Eksp. Teor. Fiz.* **77**, 114 (1979) [*Sov. Phys. JETP* **50**, 58 (1979)].
- [37] T. Georges and F. Favre, *J. Opt. Soc. Am. B* **10**, 1880 (1993).
- [38] T. Georges, *Opt. Fiber Technol.* **1**, 97 (1995).
- [39] H. Hasegawa and Y. Kodama, *Solitons in Optical Communications* (Oxford University Press, New York, 1995).
- [40] A. Hasegawa and Y. Kodama, *Proc. IEEE* **69**, 1145 (1981).
- [41] P. L. Kelley, I. P. Kaminow, and G. P. Agrawa, *Nonlinear Fiber Optics* (Academic Press, San Francisco, 2000).
- [42] E. Kengne, A. Lakhssassi, and W. M. Liu, *Phys. Rev. E* **91**, 062915 (2015).
- [43] D. Y. Tang, H. Zhang, L. M. Zhao, and X. Wu, *Phys. Rev. Lett.* **101**, 153904 (2008).
- [44] S. Liu, Z. Fu, S. Liu, and Z. Wang, *Chaos Solitons Fractals* **19**, 795 (2004).
- [45] A. M. Dikandé, *Phys. Rev. A* **81**, 013821 (2010).
- [46] A. M. Dikandé, *J. Opt.* **13**, 035203 (2011).
- [47] A. M. Dikandé, *Phys. Scr.* **60**, 291 (1999).
- [48] D. Toko, R. L. Woulache, C. B. Tabi, L. Kavitha, A. Mo-hamadou, and T. C. Kofane, *J. Phys. Chem. Biophys.* **3**, 1000112 (2013).
- [49] X. Li, J. Wang, and W. Hu, *Phys. Rev. E* **76**, 041902 (2007).
- [50] E. A. E. Akova, E. E. Shnol, M. A. Panteleev, A. A. Butylin, V. Volpert, and F. I. Ataulakhanov, *Model. PLoS ONE* **4**, e4454 (2009).
- [51] J. Wojcik and A. Shilnikov, *Physica D* **240**, 1164 (2011).
- [52] F. Bowman, *Introduction to Elliptic Functions with Applications* (Dover, New York, 1961).
- [53] M. S. Baptista, F. M. Moukam Kakmeni, and C. Grebogi, *Phys. Rev. E* **82**, 036203 (2010).
- [54] T. B. Benjamin and J. E. Feir, *J. Fluid Mech.* **27**, 417 (1967).
- [55] D. S. M. Petmegni and A. M. Dikandé, *J. Mod. Opt.* **64**, 1192 (2016).
- [56] A. E. Hady and B. B. Machta, *Nat. Commun.* **6**, 6697 (2015).
- [57] H. Barz, A. Schreiber, and U. Barz, *Med. Hypoth.* **81**, 768 (2013).
- [58] D. E. Pelinovsky, Y. S. Kivshar, and V. V. Afanasjev, *Physica D* **116**, 121 (1998).
- [59] S. S. Mirra and B. T. Hyman, Ageing and Dementia in *Greenfield's Neuropathology*, 7th ed., edited by D. I. Graham and P. L. Lantos (E Arnold, London, 2002), pp. 195–271.
- [60] M. Uddin, S. Haq, and M. Ishaq, *Appl. Math. Sci.* **6**, 2403 (2012).
- [61] A. Salupere, *Applied Wave Mathematics* (Springer, Heidelberg, 2009).
- [62] R. H. Steele, *Arch. Bio-Chem. Biophys.* **411**, 1 (2003).
- [63] G. H. Pollack, *Cells, Gels and the Engines of Life* (Ebner and Sons, Seattle Washington, 2001).
- [64] G. N. Ling, *A Revolution in the Physiology of the Living Cell* (Krieger, Malabar, FL, 1992).